Boundary flow on end-grafted PEG brushes

Eric Charrault,[1,2] Thomas Lee[1,3], Christopher D. Easton[4] and Chiara Neto[1]*

[1]School of Chemistry F11, The University of Sydney NSW 2006, Australia

[2] Now at Future Industries Institute, University of South Australia, Mawson lakes SA 5095, Australia

[3] Now at the Department of Civil and Environmental Engineering, Massachusetts Institute of Technology, Cambridge, MA, 02139, USA

[4] CSIRO Manufacturing Flagship, Bag 10, Clayton South, Victoria 3169, Australia

* Corresponding author: chiara.neto@sydney.edu.au

KEYWORDS. Self-assembled monolayer, polymer brush, PEG, PEO, cloud-point, interfacial slip length, boundary condition, hydrodynamic force curves, penetration length

Abstract

We investigated the boundary conditions for flow of a Newtonian liquid over soft interfaces by measuring hydrodynamic drainage forces with colloid probe atomic force microscopy in a viscous liquid. The investigated soft surfaces are end-grafted brushes of thiolated poly(ethylene glycol) (PEG), of molecular weight 1k and 30k, grafted-to gold. The conditions for brush preparation were optimized as to meet the stringent conditions required for surface force measurements, namely reproducible and uniform surface composition and roughness. The fit of a slip model to the experimental data returned a slip length of 16 nm on the PEG 1k brush and 25 nm on the PEG30k brush. The slip length can be interpreted as a penetration length, which accounts for flow within the top half of the brush for the PEG30k case, and within the brush and surface roughness for the PEG1k case. These findings confirm earlier simulation studies by our group on the flow of liquids within polymer brushes.

1 Introduction

When a Newtonian liquid flows over a stationary solid surface, traditionally a no-slip boundary condition is applied at the surface, and this assumption has successfully explained most macroscopic observations (for reviews please see [1, 2]). However, over the past decade, investigations in nanoscale flows have revealed that partially wetting surfaces indeed allow liquids to slip. In the case of rigid superhydrophobic surfaces, slip greatly increases the rate of fluid flow, potentially resolving the issue of the very high hydrodynamic drag in microfluidic devices.[3]

Most of the published work on slip involves rigid interfaces, while very little work has been dedicated to slip over soft and deformable interfaces, despite the fundamental importance to understanding flow in biological confined systems. For example, the flow of blood through capillaries involves the flow of a liquid containing soft blood cells confined on the microscale between soft surfaces. It has been shown that the resistance to blood flow in capillaries is lower than would be expected based on the bulk viscosity of blood.[4] In the engineering field, it is fairly well established that soft surfaces are capable of reducing the growth of disturbances in a laminar boundary layer and thus possess the potential for reducing drag in turbulent flow.[5] For example, the skin of several aquatic animals is textured with cilia, which have the effect of reducing interfacial drag while swimming.[6] The key to understanding flow in many biological systems and around microorgansims[7] could lie in our ability to describe the boundary conditions for flow at soft surfaces.

In this study the boundary conditions for flow were investigated on soft surfaces, made of polymer brushes grafted to a substrate. Grafted polymer brushes are widely used as a chemically robust and versatile way to tailor the functional properties of surfaces, such as wettability,[8, 9] biocompatibility,[10, 11] and lubrication. [12-15] When exposed to external stimuli, such as change in temperature, pH, and salt concentration, their density and molecular conformation can be

reversibly switched.[16, 17] However, the preparation of controlled and reproducible surfaces for force measurements is challenging, and the analysis of the raw hydrodynamic measurements is more complicated than with rigid surfaces. The soft compliance of the polymer layer is indeed a sensitive parameter to take into account for slip measurements. To date, only few experimental studies have specifically investigated hydrodynamic flow on polymer grafted surfaces.[18, 19] McLean et al. investigated hydrodynamic forces between layers of physisorbed Pluronics,[18] but it has been shown that physisorbed chains are not able to sustain mechanical and environmental stresses, and undergo changes in the surface properties and grafting density over time.[20, 21] Relatively more simulation studies exist investigating slip on polymer brushes. Our group has recently used molecular dynamics simulations of short-chain polymer brushes under a Couette flow to show that the length of penetration of the flow increases with the increase in the distance between two chain grafting points.[22] Some recent works on an important biophysical system, the dendothelial glycolax filaments, which covers the blood vessels, highlighted that despite apparent similarity with grafted polymer brushes, they behave differently when subjected to a shear flow [23] and highlighted the importance of the polymer stiffness on the fluid flow [24]

In this study, we investigated the flow of a Newtonian liquid (sucrose solution) over surfaces bearing end-grafted brushes, made of either short or long poly(ethylene glycol) (PEG) chains, using colloid probe atomic force microscopy (AFM). Grafted polymer brushes were achieved in a rapid and straightforward way by "grafting to",[17] exploiting the affinity of thiol groups for gold surfaces, which leads to a covalent bond between the chain and the surface.[25, 26] They were grafted under poor solubility conditions, above the cloud-point of the polymer solution[27], to achieve a higher density of grafted chains by using the reduction of the polymer hydration shell. Although thiolated-PEG brushes have been prepared before[12, 28, 29], we report the exact conditions required for the preparation of a reproducible PEG brush surface to be used in surface force measurements, i.e. with uniform and reproducible surface composition and roughness, known on the nanoscale.

In particular, we highlight the effect of preparation conditions on surface contamination and degradation, such as the ageing of the thiol-gold bond upon exposure to normal lab conditions, the presence of salt and physisorbed polymer deposits on the surface which take hours to dissolve, and the etching of the gold from commonly used reducing agents, such as TCEP.

Our group has recently dedicated significant attention to developing reliable and reproducible measurements and analysis of interfacial slip on rigid surfaces,[30-33] and here we expand this analysis to soft interfaces, presenting results which match well our molecular dynamic simulations on similar brush systems.[22]

2 Experimental Section

Sample Preparation. Gold substrates (silicon wafer coated with chromium (20 nm) and gold (150 nm), MTI (USA)) had RMS roughness R_q = 1.10 nm as measured by AFM over 10 μm^2. Prior to grafting, the substrates were immersed and sonicated in a solution of ethanol/acetone (1:1) for 5 min, then treated for 2 min with air plasma (Harrick Plasma, Itacha NY, model PDC-002) to remove all traces of organic contamination.

PEG Self-assembled monolayer formation. Thiolated poly(ethylene)glycol (PEG) molecules of molecular weight 1100 g/mol (PEG1k) and 30000 g/mol (PEG30k) were purchased from Polymer Source (Canada). Briefly, the substrates were immersed into the 5 mg/ml PEG grafting solution for 1 - 24 hours in low solubility conditions (T = 65 º C, ionic strength I.S.(K_2SO_4) = 2.9 M for PEG1k, and T = 40 º C, I.S.(K_2SO_4) = 1.8 M for PEG30k). Surfaces resulting from cloud-point grafting are hereafter denominated as: CP-PEG1k and CP-PEG30k. After grafting, the surfaces were rinsed, then immersed in Milli-Q water for at least 10 min (CP-PEG1k) and 4 hours (CP-PEG30k), to remove physisorbed salt and molecules. The equilibrium contact angle of water on both prepared PEG brushes was 33°, with low values of contact angle hysteresis (2º for PEG1k

and 7º for PEG30k). Great care was dedicated to producing end-grafted polymer surfaces without defects, and common issues identified regarding the grafting (use of reducing agent), rinsing (removal of physisorbed species) and the ageing (evolution of surface chemistry) of the polymer brushes. These issues are described below and in in greater detail in Supporting Information.

Quartz crystal microbalance A quartz crystal microbalance (QCM-D, Q-Sense model E4) was used to monitor the PEG grafting on gold-coated quartz crystal sensors (fundamental resonance frequency 5 MHz, RMS roughness 1.00 nm). Before each measurement, the QCM crystals were equilibrated in Milli-Q water until the frequency drift was less than 0.5 Hz/2 min (at least 45 min at room temperature), in order to measure the resonant frequency and the different overtones. 'Dynamic' PEG grafting was then carried out by pumping the grafting solution inside the flow modules at flow rates in the range of 0.014 - 0.1 mL/ min for 1 - 4 hours. 'Static' PEG grafting was also performed, by stopping the flow after filling the chamber with the grafting solution. The whole measurement was performed under temperature control (25 ºC to 45 ºC). Prior to pumping into the flow chamber all solutions were maintained at a temperature 2 ºC higher than the temperature set inside the flow module, and degassed just prior to injection. The total adsorbed mass was quantified using the Sauerbrey equation using the 7th harmonic for the PEG1k system, and by modelling with a viscoelastic Voigt model for the PEG30k system.

Atomic force microscopy – Imaging: A Multimode 8 AFM (Bruker) was employed to image the surfaces in air using the Quantitative Nanomechanical Mapping (QNM) mode and a scanasyst-air probe from Bruker. -*Hydrodynamic force curves:* An Asylum MFP-3D atomic force microscope was used to measure hydrodynamic forces using the colloidal probe technique.[34] Briefly, a silica microsphere, with radius R (≈ 10 µm) measured by scanning electron microscopy (SEM), was glued onto the end of a tipless cantilever (µMash, 37 series, cantilever B). Spring constant values between 0.3 and 0.4 N/m were determined by the thermal noise method.[35] Prior to mounting the

closed liquid cell in the AFM, all the parts involved in the study were thoroughly cleaned by air plasma cleaner (when possible) or by sonication in an ethanol bath. The solution used, a 33% (wt.) aqueous sucrose solution containing 0.2 M NaCl to suppress electrostatic interactions (under these salt conditions the Debye length is round 0.8 nm)[36] was filtered with a 0.2 μm filter prior to injection in the cell. The temperature of the fluid cell was monitored and maintained at 29.0 ± 0.5 ºC for all experiments. Force measurements were taken by ramping the surfaces together over a distance of 5 - 6 μm at an approach rate of 0.1 - 80 μm/s. The acquisition of data was such that at least 2000 points were recorded during the extension-retraction run, regardless of the approach rate. The slip lengths values were averaged over three measurements separated by a waiting time of 2 min, the standard deviation was used for the error bars. The viscosity of the 33% sucrose solution used was calculated based on the work of Asadi [37] and was confirmed by shear viscosity measurement ($\eta_{sucrose\ 33\%}$ = 2.90 ± 0.02 mPa.s at 29 ºC).

3 Results

In this work we investigated the boundary conditions of flow over soft surfaces by performing drainage experiments on end-grafted PEG brushes grafted to gold substrates, called CP-PEG 1k and CP-PEG30k, grafted under cloud point conditions. In Supporting Information, we specify how the grafting and rinsing conditions needed to be optimized in order to reduce contamination and defects on the PEG brushes, and to reproducibly graft brush surfaces which are suitable for force measurements, in virtue of the reproducibility and uniformity of their surface composition and roughness. The main insights gained on the preparation of high-quality and reproducible brushes are also summarised briefly here.

Preparation of end-grafted PEG brushes

Our brush preparation combines the ease of formation of a self-assembled monolayer of thiolated polymer chains on gold and the efficiency of grafting under marginal solvation of the polymer chains (cloud point). The formation of layers of short PEG1k and of long PEG30k was assessed by a suite of complementary characterization techniques, such as contact angle measurements, X-ray photoelectron spectroscopy (XPS), quartz crystal microbalance (QCM) and AFM imaging and force measurements. After the system optimisation, the prepared PEG brushes were highly controlled and reproducible, of a quality suitable for surface forces experiments. Although the chemical procedure is straightforward, important details of the preparation procedure were identified:

i) The prepared polymer brushes need to be stored in the dark or under water, to reduce degradation of the thiol-gold bond. Both the thiolated PEG brushes degraded readily when exposed for two weeks to normal lab conditions (exposure to sunlight and oxygen), as demonstrated by more than doubling of the value of the equilibrium contact angle, changing from 33° just after preparation to above 60° (Figure S2, Supporting Information). The contact angle hysteresis also changed drastically, increasing from around 0° to around 60° in both systems. Samples exposed to long sessions of AFM imaging also showed this effect. The dramatic change in equilibrium contact angle and contact angle hysteresis of the CP-PEG30k and CP-PEG1k surfaces exposed to ambient light over time is a sign of degradation of the thiol-gold bond due to UV and oxygen exposure. Previously, alkanethiolates in self-assembled monolayers on gold have been observed to oxidize in air, in the dark, to form the corresponding sulfinates and sulfonates, which desorb from the surface.[29, 38] Our experiments showed that keeping the PEG surfaces away from all light (stored in the dark) or with reduced UV and oxygen (by immersing in a UV-adsorbing medium such as water) largely preserved the quality of the PEG layer.

ii) The CP-PEG30k surfaces need to be washed thoroughly, by immersion in water for up to 4 hours, to remove from the surface dendritic and large salt deposits. These deposits are particularly robust and strongly attached, due to the co-presence of entangled long polymer chains and a large amount of salt in the grafting solution. Short immersion times do not remove the deposits on CP-PEG30k, while they are sufficient in the case of CP-PEG1k surfaces, due to the shorter length of the polymer chains. These deposits not only locally modify the surface wettability of the CP-PEG30k brushes, but also add significant roughness, which is undesired in surface force measurements (Figure S1, Supporting Information).

iii) Reducing agents are often added to thiols, to reduce the formation of disulfide bridges between the thiolated polymer chains.[39] We showed that the reducing agent tris(2-carboxyethyl)phosphine (TCEP) etches away the surface of the gold, increasing dramatically the RMS roughness of the CP-PEG30k from 0.9 nm to around 7 nm, with a large peak-to-valley value of at least 50 nm (Figure S3, Supporting Information). This dramatic increase in roughness is undesirable in surface force measurements, and so use of reducing agents should be avoided in gold-thiol systems when the potential presence of disulfide bridges is not a serious issue for the experiment.

Mass and swelling of grafted PEG brushes

Quartz crystal microbalance with dissipation (QCM-D) is a powerful technique to investigate dynamic adsorption processes at interfaces, and can determine molecular deposition with a resolution of tens of nanograms as well as detect conformation of molecules at the interface. [40] The shift in frequency of the oscillating sensor measured upon adsorption is proportional to the mass bound to the sensor, and the dissipation signal relates to the viscoelastic behavior of the deposited film (also related to the polymer's conformation). **Figure 1(a**) shows the results of a QCM experiment on the dynamic grafting of PEG1k below cloud point at 25ºC and I.S. = 0.6 M.

The sequence of liquids injected into the flow module was the following: i) Milli-Q water, ii) PEG1k grafting solution (I.S. = 0.6 M), iii) Milli-Q water. Cloud point grafting could not be achieved for PEG1k, as the maximum safe temperature in the Q-Sense QCM (45 ºC) was not high enough (cloud point in these conditions is higher than 70ºC). **Figure 1**(b) shows the result of a QCM experiment on the dynamic grafting of PEG30k above the cloud point (CP-PEG30k); the sequence of liquids pumped into the flow chamber was the following: i) Milli-Q water, ii) K_2SO_4 solution (I.S. = 1.8 M), iii) PEG30k grafting solution (I.S. = 1.8 M), iv) K_2SO_4 solution (I.S. = 1.8 M), v) Milli-Q water. For clarity, only the 3rd, 5th and 7th harmonics are shown.

Both experiments were successful in grafting PEG on the gold surface, as indicated by the negative frequency shifts measured between the start and the end of the runs. After an effective grafting time of about 2 hours, the final frequency shift in the case of PEG1k was $\Delta f \approx$ -20 Hz, and in the case of CP-PEG30k was $\Delta f \approx$ -200 Hz. As observed by the plateau values reached in the frequency and dissipation shift curves during grafting, the adsorption process was fully completed (under those experimental conditions) for CP-PEG 1k (region ii), whereas the system was not stabilized for CP-PEG30k, as both frequency and dissipation shift curves were still evolving (region iii). The large steady increase in dissipation shift (t < 6000s) could be attributed to the aggregation/entanglement of the collapsed polymer chains with the adsorbed chains on the surface.

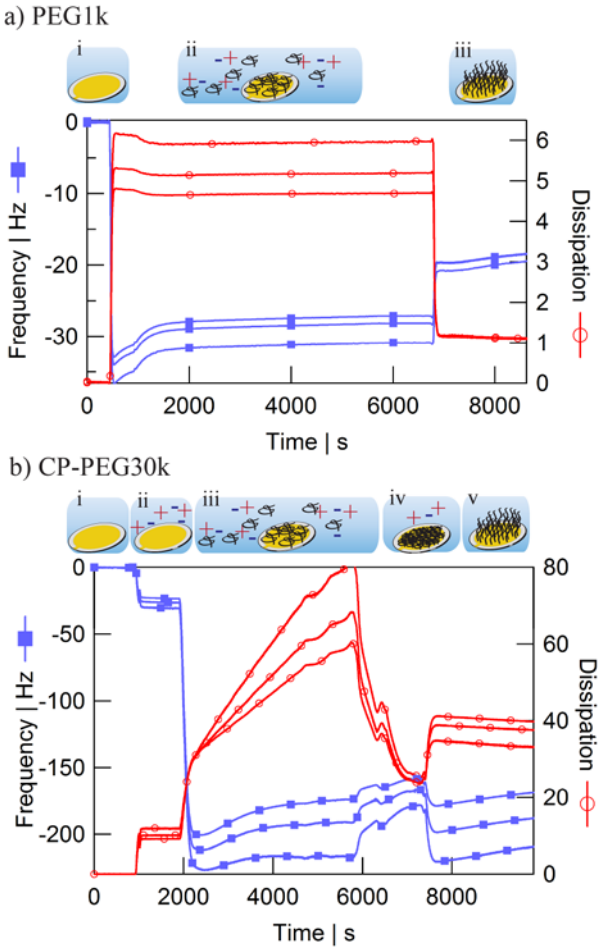


Figure 1: Dynamic QCM experiments on the grafting of PEG on gold: a) PEG1k grafting at 25ºC. The order of injections was: i) Milli-Q water, ii) PEG1k grafting solution (I.S. = 0.6 M), iii) Milli-Q water. b) CP-PEG-30k grafting at 45ºC. The order of injections was: i) Milli-Q water, ii) K_2SO_4 solution (I.S. = 1.8 M), iii) PEG30k grafting solution (I.S. = 1.8 M), iv) K_2SO_4 solution (I.S. = 1.8 M), v) Milli-Q water.

The final dissipation signals, after rinsing with water, indicate that the two polymer brushes behave differently: in Figure 1(b) for CP-PEG30k the change in dissipation signal is significant (1/5 of the frequency shift), and the curves of the different harmonics do not overlap. Both these observations attest the viscoelastic behaviour of the CP-PEG30k brush and its swelling by water. On the other hand, in Figure 1(a) for PEG1k the change in dissipation signal is relatively small (1/20 of the frequency shift) and the curves of the different harmonics are superimposed. Both of these observations are characteristic of a rigid solid film, similar to what can be expected for a

short alkanethiol chain forming a self-assembled monolayer on the surface. [41] The mass of grafted CP-PEG30k after rinsing (part v) was calculated to be m = 4200 ng/cm^2 with the viscoelastic Voigt model (with parameter values: ρ_f = 1000 kg/cm^3, υ_f =0.001 kg/ms, ρ_{L1}= 1200 kg/cm^3, υ_{L1} =0.0019 kg/ms, σ_{L1} = 10^4 Pa, t_{L1} = 92 nm, where ρ is the density, υ the viscosity, σ the elasticity, t the thickness, and the subscripts *f* an *L1* represent the fluid and the modelled layer, respectively). The Sauerbrey equation was used for PEG1k and resulted in a grafted mass of 320 ng/cm^2, based on the 7th harmonic.

Figure 1(b) also confirms that, by exchanging the poor solvent, the K_2SO_4 solution (iv), with the good solvent, pure Milli-Q water (v), the size of the polymer hydration shell of the PEG30k chains increased. This change was observed in the dissipation signal as the different harmonic curves were initially superimposed (iv), with the polymer in a collapsed state, and then became distinct, with the polymer chains being hydrated again (swelling of the brush, v). This demonstrates that different hydration levels of the polymer chains result in different polymer conformation states. [42]

AFM height micrographs of both CP-PEG1k and CP-PEG30k obtained via QNM imaging are depicted in **Figure 2.** No significant information was obtained from modulus mapping of the surfaces, but the roughness information is crucial for surface force measurements. The grainy appearance of the surface is typical of the roughness of the underlying gold layer, but on the PEG brush many small dots and connecting lines are observed between the gold grains, which are consistent with the appearance of the polymer chains. In the collapsed state the radius of gyration is r_g(PEG1k) = 0.54 nm and r_g(PEG30k) = 2.96 nm (Rg = a x $N^{0.5}/6^{0.5}$, calculated using a persistence length of the PEG monomer a = 0.278 nm [43] and N number of monomers = 23 and 682, for PEG1k and PEG30k, respectively). The density of lines and dots is significantly higher for CP-PEG30k in Figure 2(b) than for CP-PEG1k in Figure 2(a). The RMS roughness was measured at 0.9 nm on both surfaces over a scan size of 2 µm × 2 µm, and is of the same order of

magnitude than that measured for a bare gold substrate (0.8 nm, cf SI Figure S4). The peak-to-valley r_{max} values were similar for both cases and were around 10 nm.

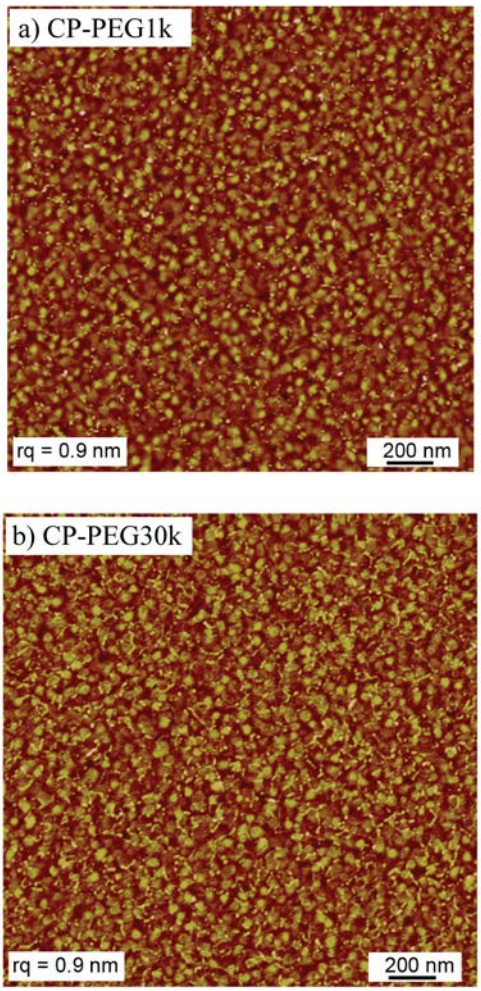


Figure 2: AFM micrographs obtained by QNM imaging in air. a) CP-PEG1k brush layer on gold, and b) CP-PEG30k brush layer on gold. The RMS roughness values corresponding to each image are shown. The vertical scale bar is 7 nm for both micrographs.

3.1 Equilibrium force measurements

In order to establish the value of the hydrodynamic thickness of the PEG brushes, equilibrium force curves were acquired at low approach rates (100 nm/s) between a silica probe and CP-PEG surfaces in a 33% sucrose solution containing 0.15 M NaCl. The onset of the repulsive forces, occurring when the colloid probe started to compress the polymer layer, was used to calculate the brush thickness. The value of the brush thickness was essential to the analysis of the hydrodynamic data, as unperturbed polymer brush thickness was used as the reference surface from which the

interfacial slip was measured. The normalized interaction forces as a function of separation are depicted in **Figure 3** for both CP-PEG1k and CP-PEG30k.

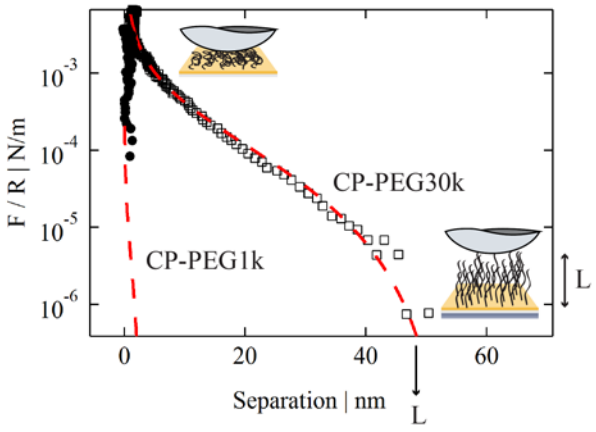


Figure 3: Semi-logarithmic normalized force profiles as a function of the separation between gold coated CP-PEG30k (empty black squares) and CP-PEG1k (filled black circles) surfaces and a silica probe. Theoretical curves of brush compression force profile as predicted by the MWC model (dashed red line) are represented for CP-PEG30k. The MWC theory, using the parameters brush thickness L = 3 nm and L = 50 nm, s = 1.5 nm and s = 14 nm, describes well the force curves for CP-PEG1k and CP-PEG30k.

Both curves are well fitted by the asymmetric[44] Milner-Witten and Cates (MWC) model[45]

$$\frac{F_{MWC,asymm(D)}}{2\pi R} = \frac{k_b T L_c}{4}\left(\frac{\pi^2 l_p}{12 s^{10}}\right)^{1/3}\left[\left(\frac{D}{L}\right)^{-1} + \left(\frac{D}{L}\right)^{2} - \frac{1}{5}\left(\frac{D}{L}\right)^{5} - \frac{9}{5}\right] \quad (1)$$

where k_b is the Boltzman constant, T the temperature, D the surface separation, L_c the contour length; fitted parameters values were: s (interchain distance) = 1.5 nm for CP-PEG1k and s = 14 nm for CP-PEG30k, and L (thickness) = 3 ± 2 nm for CP-PEG1k, and = 50 ± 5 nm for CP-PEG30k. For the CP-PEG30k system, the best fits were obtained by shifting the force curve by 3 nm, distance similar to the length of the fully squeezed polymer layer under compression. The dry polymer brush thickness value could not be measured by ellipsometry due to measurement

artefacts, related to and the optical properties of the gold substrate. An XPS dry thickness of 6 nm was calculated for CP-PEG30k using a standard XPS overlayer algorithm (Table S1 in Supporting Information) [46] Considering this dry thickness, the resulting interchain distance was calculated at 2.7 nm and led to the use of a prefactor (commonly used in scaling theory) of 0.004 in the MWC model to fit the force curve. The values of interchain distance calculated from all three sets of data for both PEG1k and PEG30k are in agreement with a brush polymer conformation[27], as they are significantly lower than the Flory radius r_f of the polymers ($2*r_f$ = 3.6 nm and 28 nm for PEG1k and PEG 30k, respectively, using $r_f = a \times N^{0.6}$). Considering the CP-PEG30k brush thicknesses from both the QCM and force curve measurements, we can hypothesize that the sucrose/salt solution is not as a good a solvent as water for our polymer. Indeed, the polymer layer thickness was estimated at 92 nm in a good solvent (water from the QCM data) and it was only estimated at around 50 nm in the sucrose mixture (from the force curve measurement). On the other hand, the dry thickness of the brush (under vacuum) is only 6 nm, so sucrose/salt solution is estimated to be still of reasonable quality for the brush.

3.2 Hydrodynamic forces on polymer brushes

The hydrodynamic force data was analysed following the procedure presented in our earlier publications.[30, 31] Briefly, experimental force data was fitted with both a no-slip model and a slip model, and the slip length was obtained from the fit of the slip model to the experimental force (other forces such as the drag force on the cantilever and van der Waals forces were taken into account). Before the slip fit, each force curve was analysed individually to set the zero of separation, calculate the compliance value, and the spring constant value. The spring constant was obtained by three separate methods, and a comparison made, see Table 1. In the hydrodynamic method, the experimental force was fitted by the no-slip model at large separations (typically from 1.3 to 2 um).[30, 47] Then an average value of the spring constant was calculated over a range of rates (typically between 30 and 60 um/s). As shown in Table 1, the spring constant values obtained

from the hydrodynamic method were in very good agreement with the values obtained by thermal noise calibration[35] and the Sader method.[48]

	thermal noise[35]	Sader method[48]	hydrodynamic fit[30, 47]
spring constant (N/m)	0.367 ± 0.017	0.361 ± 0.010	0.360 ± 0.048

Table 1: Cantilever spring constant calibration. The spring constant value determined by hydrodynamic fit of the force curve relates to the intrinsic value as defined in [49]

The employed slip model was the one by Vinogradova, which describes the hydrodynamic drainage force on a sphere approaching a flat surface under the slip boundary condition: [50]

$$F_h = \frac{-6\pi\eta R^2 \dot{h}}{h} f^* \quad (h << R), \tag{2}$$

where η is the viscosity of the liquid, R is the radius of the microsphere, $\dot{h}$ is the velocity of the microsphere relative and perpendicular to the substrate, h is the distance of closest approach of the sphere surface to the substrate surface, and f^* is the correction factor for slip at two surfaces with the same slip length b; a no-slip model is obtained when $f^* = 1$:

$$f^* = \frac{h}{3b}\left[\left(1+\frac{h}{3b}\right)\ln\left(1+\frac{6b}{h}\right)-1\right] \tag{3}$$

The main difference between a solid substrate and a surface bearing polymer brushes is the presence of an interfacial layer with softer compliance. This layer can be squeezed upon approach of the colloid probe and can affect the resulting force profile in many ways. First of all, an extra compression force arises when the probe squeezes the polymer layer [51, 52]. Secondly, it is likely that at high rates of approach the hydrodynamic force is large enough to compress the brush while the probe is not in contact with it.[53] Finally, the choice of reference plane for slip is not obvious on soft surfaces. In AFM force experiments, the zero of separation and hard contact between the

surfaces is obtained when the probe cannot squeeze the brush anymore, and one-to-one coupling between piezo movement and cantilever deflection is achieved (the hard compliance region). However, before hard compliance is reached, there is a region of the force curve in which at the same time the probe compresses the brush and liquid is able to flow within the brush. Indeed, based on earlier work by the Granick group, it is expected that as the separation between the polymer brush coated surfaces decreases, the apparent slip plane moves closer to the solid surfaces.[53, 54] In order to overcome these issues, the experimentally measured curves were fitted with the hydrodynamic models only down to a separation equal to the hydrodynamic thickness of the polymer brush (50 nm for CP-PEG30k and 3 nm for CP-PEG1k, as obtained by equilibrium force measurements, Figure 3). A similar approach was used in earlier works for the description of hydrodynamic and lubrication forces on surfaces bearing adsorbed species.[55, 56] By doing so, a 'soft contact point' is chosen as the zero of separation and our reference surface for slip, instead of the usual hard contact point which would be obtained when the polymer brush is fully squeezed. The fit of the experimental data to the slip model is taken to indicate the amount of interfacial slip on top of an unperturbed polymer brush, explicitly ignoring the polymer brush compression due

to hydrodynamic forces.[53] This simplification could lead to a slight overestimate of the slip length values measured at high approach rates.

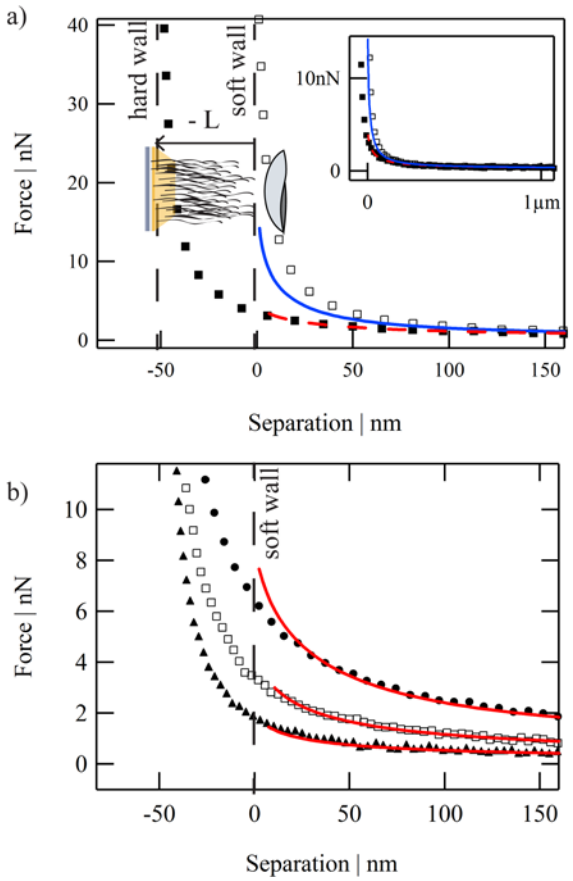


Figure 4: a) Hydrodynamic force curves for CP-PEG30k measured at 20 µm/s. The extension force curve (empty squares) is shifted by the estimated polymer brush thickness (filled squares). The no slip model (blue line) and the slip model (dashed red line) are fitted to the extension and shifted extension curves, respectively. b) Hydrodynamic forces measured at 20 µm/s (triangles), 50 µm/s (empty squares) and 80 µm/s (circles), shifted by the estimated polymer brush thickness (hard wall at -50 nm). The solid red lines are the corresponding fits to the slip model.

Figure 4a presents the hydrodynamic force measured on a CP-PEG30k brush upon approach of the colloid probe. The empty squares are experimental values obtained using the hard wall, i.e. the fully squeezed brush in contact with the colloid probe, as zero of separation. The empty squares lay significantly above the no-slip model, hence this hydrodynamic force curve which cannot easily be fitted, would result in a negative slip length. The filled squares represent the same force data shifted to the left by the thickness of the unperturbed polymer brush (50 nm), using the 'soft wall', i.e. the top of the polymer brush, as zero of separation. This shifted force curve could be

well fitted with the hydrodynamic slip model,[50] and gave a fitted slip length of 32 nm. Shifting the zero of separation to the soft wall allows us to use the commonly used slip model, using the top of the brush as reference slip plane, and to draw similarities with results on hard surfaces.

Figure 4b shows similarly shifted force curves at different approach rates and their corresponding slip fits. The fit with the slip model is good at most approach rates, and the fitted slip length versus approach rates are shown in **Figure 5**. The slip length is largely independent of the approach rate, as previously observed.[32] The agreement between the shifted experimental data and the slip model is not as good at the highest approach rate (80 μm/s). This could be an indication that the polymer layer is partially squeezed before contact with the probe at this higher hydrodynamic force, and this could result in an overestimate of the slip length value. Similar results, with slightly smaller slip length values, were obtained on the CP-PEG1k brush, as reported in Figure 5. Due to their short polymer brush, the CP-PEG1k surface analysis did not required the shift of the compressed layer.

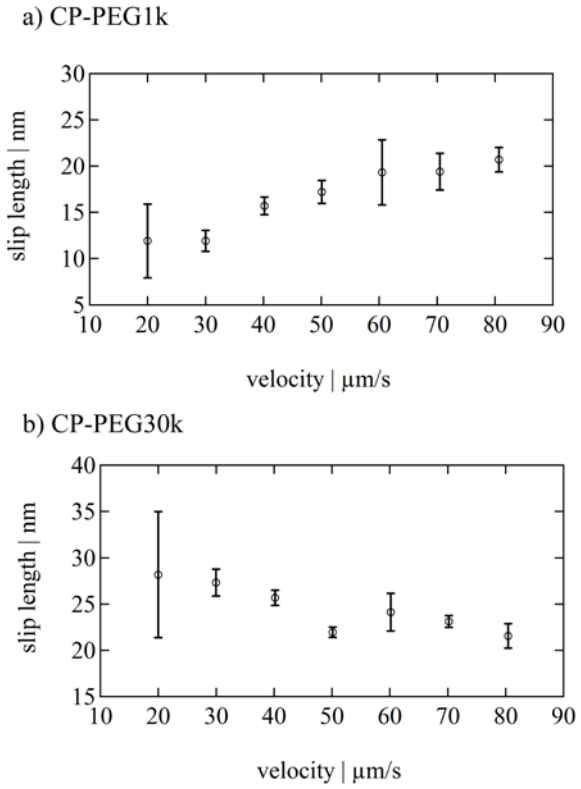


Figure 5: Average fitted slip lengths versus approach rates obtained on a) CP-PEG1k brush surface; b_{mean}=16 ± 4 nm; and b) CP-PEG30k brush surface ; b_{mean}=25 ± 3 nm. The error bars represent the standard deviations calculated on several force curves over two/three different contacts. The error due to uncertainty of the polymer brush thickness is ± 5 nm.

As shown in Figure 5, the fitted values of slip length show very slight variation upon change in approach rate, largely within the standard deviation. The variation is mainly due to an imperfect fit of the spring constant (the same average value of spring constant is used for all force curves). The fitted slip length value averaged over all approach rates is 16 ± 4 nm for CP-PEG1k and 25 ± 3 nm for CP-PEG30k, with a significantly higher slip on the thicker brush. By intentionally not shifting the CP-PEG1k force curve by the polymer thickness (a few nm), we are underestimating the interfacial slip values. Values resulting from such analysis (data not shown) showed that the reduction in slip is not significant and within the experimental error. [57]

The two CP-PEG grafted surfaces exhibit similar surface chemistry, but behave rather differently in terms of slip. **Figure 6** illustrates the mechanism that could lead to slip on these two PEG surfaces. For CP-PEG1k (Figure 6(a)), the thickness of the polymer brush (3 nm) is smaller than the peak-to-value roughness value of the gold substrate (r_{max}= 10 nm). Upon approach of the probe, the polymer brush is squeezed and the liquid is still able to flow within the deep valleys of the substrate. The average slip value calculated for the CP-PEG1k (b = 16 nm) is close to the peak-to-valley roughness value of the substrate (10 nm). This interpretation has been proposed before to explain the slip of liquids over rough substrates.[3]

For CP-PEG30k (Figure 6(b)), the thickness of the polymer brush (50 nm) is much larger than the peak-to-valley roughness of the gold substrate, so the roughness alone cannot account for the observed slip in this case. In this case, the fitted slip length b = 25 nm is interpreted as a penetration length l_p, the distance the liquid flow penetrates into the brush. This penetration length also defines a stagnation length l_s, which describes the portion of the grafted brush that is not affected by the fluid penetration, and is effectively a hydrodynamic measure of brush height, ($l_s = L - b$ = 25 nm). In the CP-PEG30k case, the liquid appears to penetrate approximately half of the brush thickness, and this mechanism agrees with the established knowledge that the brush density is higher close to the grafting points on the substrate than on the top of the brush.[58]

These experimental results are in good qualitative agreement with coarse-grained non-equilibrium molecular dynamics simulations recently conducted in our group.[22] We reported the results of simulations which showed that the flow of the solvent penetrated significantly into the outer regions of the brush. As grafting density was increased, the physical thickness of the brush measured from the density profile scaled in proportion with s^{-2}, provided that the exponential tail in the density profile at the top of the brush was taking into account. The hydrodynamic thickness, l_s, increased more gradually, in proportion with $s^{-2/3}$, leading to a penetration length which increased monotonically with decreasing grafting density.

The molecular simulations also demonstrated that the collapse of the brush when changing the solvent quality from a good to poor dramatically changed the boundary condition. The boundary condition of the poor solvent state is complicated by the fact that depending on the grafting density the polymer may collapse into discrete aggregates, leaving areas of the underlying substrate exposed. The morphology of these patterns depends strongly on the grafting density and the amount of solvent adsorbed in the brush.[22] The collapse therefore creates nanoscale surface roughness and chemical heterogeneities, both of which will influence the apparent slip length.[22] The simulation results indicate that the boundary condition in a poor solvent will depend on the grafting density because of the effect of grafting density on the morphology of the pattern, which would not be the case if the brush collapsed homogeneously at all grafting densities.

Our colloid probe AFM measurements are well suited to test the molecular dynamics result, as both the physical and hydrodynamic height can be measured in the same experiment. Equilibrium force curves provide a density measurement of the brush thickness (50 nm for PEG30k), while hydrodynamic force curves provide the hydrodynamic thickness of the brush (25 nm). These results confirm there is a significant difference between the physical and hydrodynamic thickness, and that the penetration length is non-zero and positive. In terms of interfacial slip, these results indicate that in laminar flow a soft, complaint surface does not appear to increase interfacial slip and reduce reducing drag, as has been suggested in turbulent flow. However, the slip effect is expected to become more important when the wettability of the brush by the liquid is decreased,[22] and studies along these directions are under way.

Our controlled and reproducible PEG system is ideally suited to mirror the molecular dynamics simulations in testing the effect of brush grafting density on interfacial slip. The grafting density can be gradually reduced by grafting the polymer in solvents of increasingly higher quality.[59] The solvent quality can be finely tuned by changing the grafting solution temperature and ionic strength. Once the polymer is grafted, the density of the brush can be reversibly changed by

changing the temperature of the system, and force curves can be performed both in the collapsed state and in the swollen state. This will allow comparison with our molecular simulation result, which predicts that changes in grafting density will impact on the slip length due to differences in the patterns formed on collapse of the brush.

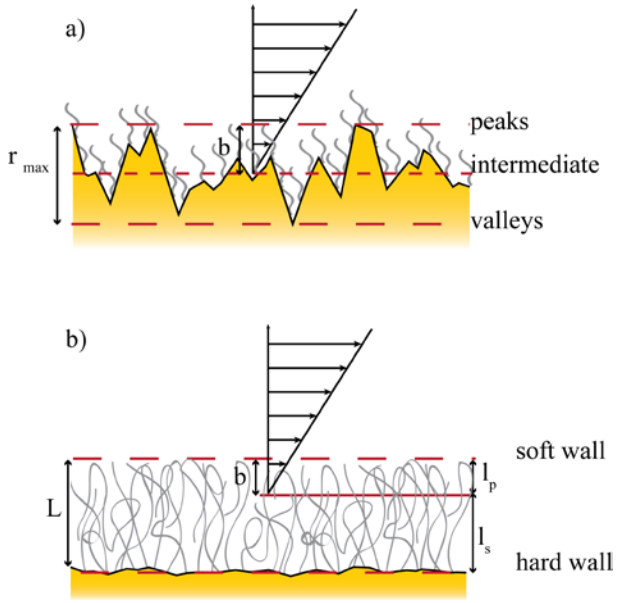


Figure 6: Mechanism for slip on polymer brush surfaces for a) CP-PEG1k, and b) CP-PEG30k. On a rough and soft surface the definition of slip depends on where the reference plane is chosen.

4 Conclusions

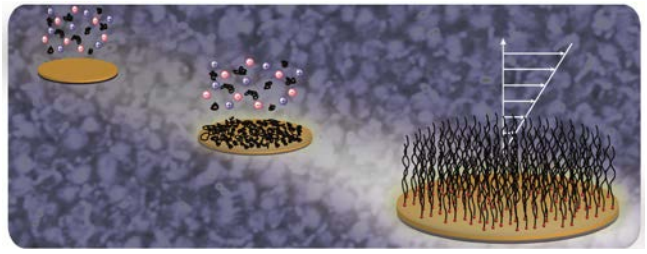
We were able to prepare end-grafted PEG brushes on gold and optimise the preparation conditions so that the surfaces were highly controlled and reproducible, of a quality suitable for surface forces experiments. The interfacial slip of a Newtonian liquid on a soft layer made of a grafted polymer brush was investigated. By shifting the force curve by the length of the unperturbed polymer brush, we were able to fit the force curves with a slip model, using the soft wall as the reference surface. Interfacial slip values of around 16 nm were measured on a 3 nm thick PEG brush and 25 nm on a 50 nm thick brush. On the thin polymer brush, with thickness equivalent to the peak-to-valley

roughness of the underlying substrate, slip is controlled by the surface roughness, whereas for thicker polymer brush, the penetration of the fluid into the brush dictates the magnitude of the slip length.

ACKNOWLEDGEMENT

The authors thank Dr. Phil Attard for useful discussions on the nominal spring constant calculation, and acknowledge the Australian Research Council for funding (DP110101533).

TOC



REFERENCES

1. C. Neto, D. R. Evans, E. Bonaccurso, H.-J. Butt and V. S. J. Craig, *Rep. Prog. Phys.*, 2005, **68**, 2859-2897.
2. T. Lee, E. Charrault and C. Neto, *Adv. Colloid Interface Sci.*, 2014, **210**, 21-38.
3. H. Ouyang, Z. Xia and J. Zhe, *Microfluid Nanofluid*, 2010, **9**, 915-922.
4. T. W. Secomb, R. Hsu and A. R. Pries, *Proc. Inst. Mech. Eng., Part J*, 2006, **220**, 767-774.
5. K. S. Choi, X. Yang, B. R. Clayton, E. J. Glover, M. Atlar, B. N. Semenov and V. M. Kulik, *Proceedings of the Royal Society of London A: Mathematical, Physical and Engineering Sciences*, 1997, **453**, 2229-2240.
6. D. W. Bechert, M. Bruse, W. Hage and R. Meyer, *Naturwissenschaften*, 2000, **87**, 157-171.
7. E. Lauga and T. R. Powers, *Reports on Progress in Physics*, 2009, **72**.
8. M. Motornov, S. Minko, K. J. Eichhorn, M. Nitschke, F. Simon and M. Stamm, *Langmuir*, 2003, **19**, 8077-8085.
9. A. Sidorenko, S. Minko, K. Schenk-Meuser, H. Duschner and M. Stamm, *Langmuir*, 1999, **15**, 8349-8355.
10. A. M. Telford, L. Meagher, V. Glattauer, T. R. Gengenbach , C. D. Easton and C. Neto, *Biomacromolecules*, 2012, **13**, 2989–2996.
11. A. M. Telford, C. Neto and L. Meagher, *Polymer*, 2013, **54**, 5490-5498.
12. R. Heeb, S. Lee, N. V. Venkataraman and N. D. Spencer, *ACS Appl. Mater. Interfaces*, 2009, **1**, 1105-1112.
13. F. T. Limpoco, R. C. Advincula and S. S. Perry, *Langmuir*, 2007, **23**, 12196-12201.
14. J. Klein, *Annu. Rev. Mater. Sci.*, 1996, **26**, 581-612.
15. R. C. Advincula, W. J. Brittain, K. C. Caster and J. Ruhe, *Polymer Brushes: Synthesis, Characterisation, Applications*, Wiley-VCH, Weinheim, Germany, 2004.
16. R. Barbey, L. Lavanant, D. Paripovic, N. Schuwer, C. Sugnaux, S. Tugulu and H. A. Klok, *Chem. Rev.*, 2009, **109**, 5437-5527.
17. B. Zdyrko and I. Luzinov, *Macromol. Rapid Commun.*, 2011, **32**, 859-869.
18. S. C. McLean, H. Lioe, L. Meagher, V. S. J. Craig and M. L. Gee, *Langmuir*, 2005, **21**, 2199-2208.
19. L. Lanotte, S. Guido, C. Misbah, P. Peyla and L. Bureau, *Langmuir*, 2012, **28**, 13758-13764.
20. T. Abraham, S. Giasson, J. F. Gohy and R. Jerome, *Langmuir*, 2000, **16**, 4286-4292.
21. U. Raviv, S. Giasson, N. Kampf, J. F. Gohy, R. Jérôme and J. Klein, *Nature*, 2003, **425**.
22. T. Lee, S. C. Hendy and C. Neto, *Macromolecules*, 2012, **45**, 6241–6252.
23. M. G. Deng, X. J. Li, H. J. Liang, B. Caswell and G. E. Karniadakis, *J. Fluid Mech.*, 2012, **711**, 192-211.

24. F. Romer and D. A. Fedosov, *Europhys. Lett.*, 2015, **109**.
25. J. C. Love, L. A. Estroff, J. K. Kriebel, R. G. Nuzzo and G. M. Whitesides, *Chem. Rev.*, 2005, **105**, 1103-1169.
26. A. Ulman, *Chem. Rev.*, 1996, **96**, 1533.
27. P. Kingshott, H. Thissen and H. J. Griesser, *Biomaterials*, 2002, **23**, 2043-2056.
28. P. Kingshott and H. J. Griesser, *Curr. Opin. Solid State Mater. Sci.*, 1999, **4**, 403-412.
29. K. Jans, K. Bonroy, R. De Palma, G. Reekmans, H. Jans, W. Laureyn, M. Smet, G. Borghs and G. Maes, *Langmuir*, 2008, **24**, 3949-3954.
30. L. Zhu, P. Attard and C. Neto, *Langmuir*, 2011, **27**, 6701–6711.
31. L. Zhu, P. Attard and C. Neto, *Langmuir*, 2011, **27**, 6712–6719.
32. L. Zhu, P. Attard and C. Neto, *Langmuir*, 2012, **28**, 3465-3473.
33. L. Zhu, C. Neto and P. Attard, *Langmuir*, 2012, **28**, 7768–7774.
34. V. S. J. Craig, C. Neto and D. R. M. Williams, *Phys. Rev. Lett.*, 2001, **87**, 054504.
35. J. L. Hutter and J. Bechhoefer, *Rev. Sci. Instrum.*, 1993, **64**, 1868-1873.
36. P. Hamilton-Brown, T. Gengebach, H. J. Griesser and L. Meagher, *Langmuir*, 2009, **25**, 9149-9156.
37. M. Asadi, *Beet-Sugar Handbook*, John Wiley & Sons, Inc., 2006.
38. M. T. Lee, C. C. Hsueh, M. S. Freund and G. S. Ferguson, *Langmuir*, 1998, **14**, 6419-6423.
39. J. C. Han and G. Y. Han, *Anal. Biochem.*, 1994, **220**, 5-10.
40. M. Rodahl, F. Hook, A. Krozer, P. Brzezinski and B. Kasemo, *Rev. Sci. Instrum.*, 1995, **66**, 3924-3930.
41. K. B. Rodenhausen, B. A. Duensing, T. Kasputis, A. K. Pannier, T. Hofmann, M. Schubert, T. E. Tiwald, M. Solinsky and M. Wagner, *Thin Solid Films*, 2011, **519**, 2817-2820.
42. G. Zhang and C. Wu, *Macromol. Rapid Commun.*, 2009, **30**, 328-335.
43. P. Harder, M. Grunze, R. Dahint, G. M. Whitesides and P. E. Laibinis, *J. Phys. Chem. B*, 1998, **102**, 426-436.
44. S. Block and C. A. Helm, *J Phys Chem B*, 2008, **112**, 9318-9327.
45. S. T. Milner, T. A. Witten and M. E. Cates, *Europhys. Lett.*, 1988, **5**, 413.
46. D. F. Mitchell, K. B. Clark, J. A. Bardwell, W. N. Lennard, G. R. Massoumi and I. V. Mitchell, *Surf. Interface Anal.*, 1994, **21**, 44-50.
47. V. S. J. Craig and C. Neto, *Langmuir*, 2001, **17**, 6018-6022.
48. J. E. Sader, J. W. M. Chon and P. Mulvaney, *Rev. Sci. Instrum.*, 1999, **70**, 3967-3969.
49. P. Attard, *ARXIV*, 2012, **eprint arXiv:1212.3019**.
50. O. I. Vinogradova, *Langmuir*, 1995, **11**, 2213-2220.
51. P. G. De Gennes, *Journal De Physique*, 1976, **37**, 1445-1452.
52. S. T. Milner, T. A. Witten and M. E. Cates, *Macromolecules*, 1988, **21**, 2610-2619.
53. Y.-K. Cho, A. Dhinojwala and S. Granick, *J. Polym. Sci.: Polym. Phys.*, 1997, **35**, 2961-2968.
54. A. Dhinojwala and S. Granick, *Macromolecules*, 1997, **30**, 1079-1085.
55. J. M. Georges, S. Millot, J. L. Loubet and A. Tonck, *J. Chem. Phys.*, 1993, **98**, 7345-7360.
56. J. Klein, Y. Kamiyama, H. Yoshizawa, J. N. Israelachvili, G. H. Fredrickson, P. Pincus and L. J. Fetters, *Macromolecules*, 1993, **26**, 5552-5560.
57. C. Hall, S. Field, K. Zuber, P. Murphy and D. Evans, *Corrosion Science*, 2013, **69**, 406-411.
58. R. R. Netz and M. Schick, *Macromolecules*, 1998, **31**, 5105-5122.
59. M. Ghezzi, S. C. Thickett, A. M. Telford, C. D. Easton, L. Meagher and C. Neto, *Langmuir*, 2014, **30**, 11714-11722.